All-Fiber High Efficiency Wavelength-Tunable Mode-Locked Cylindrical Vector Beam Laser

Yuan Lu and Peijun Yao

Abstract—A wavelength-tunable mode-locked cylindrical vector beam (CVB) fiber laser with a dumbbell-shaped structure was proposed and demonstrated experimentally. A homemade broadband long-period fiber grating (LPFG) and a high-birefringence Sagnac fiber loop work as mode converter and comb filter respectively. The mode-locking mechanism is based on the nonlinear polarization rotation (NPR) effect. The central wavelength can be tuned from 1023.257 nm to 1046.123 nm with mode-locked operating state. The laser has a high slope efficiency of 15.75% with the mode-locking threshold value of 232.5 mW at the central wavelength of 1041.361 nm. The mode-locked CVB pulses have a repetition rate of 7.06 MHz with the duration of 107 picoseconds. Radially and azimuthally polarized beams can be obtained by eliminating the degeneracy of LP_{11} mode, with the purity of 94.86%. This CVB laser with controllable operating wavelength may have potential applications in mode division multiplexed (MDM) systems, optical manipulation, and electron acceleration.

Index Terms—Cylindrical vector beam, fiber laser, mode-locked laser, wavelength-tunable.

I. INTRODUCTION

CYLINDRICAL vector beams (CVBs) are vector beam solutions of Maxwell's equations, the intensity distributions of which present a donut shape and the polarization distributions have cylindrical symmetry. Compared with conventional Gaussian beams, a smaller spot size can be reached by focusing CVBs with high aperture lens [1]. And flattop focal shapes can be obtained by shaping technique using CVBs [2], [3]. These properties make it play an important role in many areas such as material processing [4], optical trapping [5], second-harmonic generation [6], biomimetic surface structuring [7], optical data storage [8], sensor [9], and so on. What's more, theory indicates CVBs outperform conventional Gaussian beams for wireless power transfer within the Fresnel zone recently [10]. The need for practical applications promotes the rapid development of techniques to produce CVBs. Passive methods are transforming Gaussian beam into CVBs by using a mode converter such as spatial light modulators [11], subwavelength gratings [12], and Q-plates [13]. Active methods are aimed for

achieving laser oscillating in higher-order mode and CVBs are emitted from the laser cavity directly [14]–[16]. LP_{11} mode in few-mode fiber contains four degenerated modes, including TM_{01}, TE_{01}, HE_{21odd}, and HE_{21even} modes. TE_{01} and TM_{01} modes correspond to azimuthally and radially polarized beams respectively, which makes it possible to produce CVBs in an all-fiber structure. In the past few years, all-fiber CVB lasers attract more and more attention due to the advantages of simple structure, good flexibility, and good heat dissipation. Moreover, all-fiber structures are helpful for combining with mode-locking techniques to generate CVB mode-locked pulses.

In 2015, Sun *et al.* achieved a mode-locked CVB fiber laser by utilizing the offset splicing structure to excite higher-order mode with a figure-8 configuration, where a few-mode fiber Bragg grating (FM-FBG) acts as transverse mode selector [17]. The laser can emit rectangular pulses with duration tunable from 2.8 to 23 ns. In 2017, Chen *et al.* demonstrated an all-fiber actively mode-locked laser producing CVB pulses with high efficiency and a tunable repetition rate, where a two-mode long-period fiber grating (TM-LPFG) was introduced into the laser cavity as a mode converter and a two-mode fiber Bragg grating (TM-FBG) is used as a mode selector [18]. In 2018, Wan *et al.* proposed a passively mode-locked CVB fiber laser using a mode selective coupler (MSC) as the transverse mode converter and a semiconductor saturable absorber mirror (SESAM) for mode-locking [19]. The pulse repetition rate is 18.58 MHz with the signal-to-noise ratio (SNR) of 52 dB. In 2019, Xu *et al.* reported a passively mode-locked all-fiber ring-cavity laser for CVB generation based on the nonlinear polarization rotation (NPR) effect, where a two-mode fiber optical coupler (TMF-OC) was used to generate CVBs [20]. In addition, CVB mode-locked laser based on mode superposition with an all-polarization-maintaining fiber structure [21] has been also demonstrated. However, these mentioned CVB fiber lasers operate at fixed wavelengths due to the relatively narrow spectral bandwidth of the mode converter or the mode selector. On the other hand, many applications such as sensing [22], [23], material handling and processing [24], [25], and optical trapping [26], [27] are sensitive to wavelength. In aspect of optical nonlinear application and study, laser with different wavelength may be required. Therefore, wavelength-tunable lasers are important which can meet the demand in different applied fields. However, wavelength-tunable CVB fiber lasers are rarely reported.

Conventional mode-locked fiber lasers based on NPR usually has a ring-cavity structure [28]–[31], where the optical isolator (ISO) or the optical circulator brings additional loss. In this
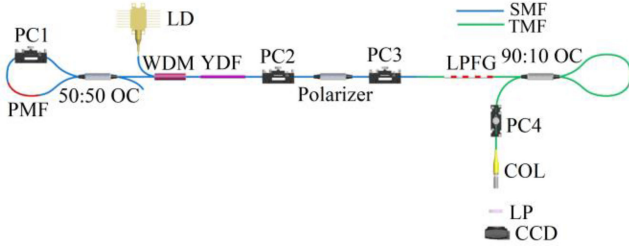
Fig. 1. Experimental setup of the wavelength-tunable mode-locked CVB fiber laser; OC, optical coupler; SMF, single-mode fiber; COL, collimator.
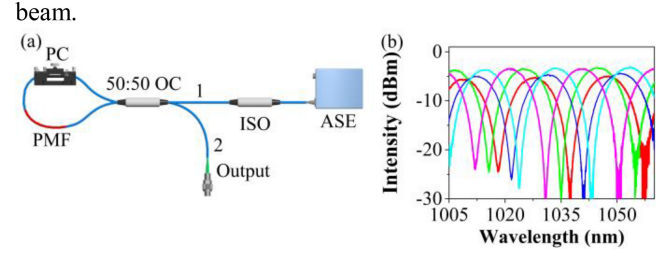

Fig. 2. (a) Measuring equipment of the Sagnac filter's transmission spectrum; (b) Measured transmission spectra of the Sagnac filter (curves of different colors correspond to different polarization states of PC1).

paper, a dumbbell-shaped NPR mode-locked fiber laser was proposed to generate CVB pulses. A broadband LPFG and a high-birefringence Sagnac fiber loop are employed as mode converter and filter respectively. By adjusting the polarization state of the polarization controller (PC) in the Sagnac filter, the laser achieves tunable wavelength range from 1023.257 nm to 1046.123 nm. Radially and azimuthally polarized beams can be switched by adjusting another PC mounted outside the laser cavity.

II. EXPERIMENT PRINCIPLE AND SETUP

The schematic of our proposed mode-locked laser with CVB generation is illustrated in Fig. 1. The Sagnac filter is composed of a 50:50 single-mode optical fiber coupler, a 12 cm polarization-maintained fiber (PMF, Nufern, PM980-XP) with the birefringence of $\sim 4.5 \times 10^{-4}$, and a PC (PC1). A 974 nm laser diode (LD) pumps a 23 cm single-mode ytterbium-doped fiber (YDF, Nufern, Yb1200) with 1200 dB/m absorption at 976 nm via a 980/1053 nm wavelength-division multiplexer (WDM). A polarizer and two PCs (PC2 and PC3) placed inside the laser cavity are used to realize mode-locked operation based on the mode-locking mechanism of NPR. The broadband LPFG fabricated using two-mode fiber (TMF) is used to convert LP_{01} mode to LP_{11} mode. A 90:10 two-mode optical fiber coupler constitutes the right Sagnac reflector, which not only acts as the right cavity mirror but also provides a 64% laser output [32]. PC4 is installed outside the laser cavity to tune the polarization state of the output modes. The numerical aperture (NA) and cutoff wavelength of the SMF (blue line in Fig. 1, Corning, HI-1060) are 0.14 and 920 nm. The diameters of core and cladding are 5.3 μm and 125 μm respectively. The spectral properties of the laser are measured by an optical spectrum analyzer (OSA, YOKOGAWA, AQ6373B). A 4 GHz oscilloscope (LeCroy, Waverunner 640Zi) together with a 3 GHz photoelectric detector is employed to record the temporal characteristics. The pulse duration is measured by an autocorrelator (A.P.E, pulseCheck 600). The mode field profiles of the output beam can be captured by a charge-coupled device (CCD, @1.0 μm) camera after been collimating. A linear polarizer (LP) is placed before the CCD to test the polarization distribution of the output beam.

The period of the transmission curves can be calculated theoretically [33],

$$\Delta \lambda = \lambda^2 / (\mathrm{BL}). \tag{1}$$

where λ is 1035 nm, B and L represent the birefringence and the length of the PMF. As a result, the period is approximately 19.84 nm. The filtering characteristics of the Sagnac filter can be measured by the experimental device shown in Fig. 2(a). An amplified spontaneous emission (ASE) source is injected into the Sagnac filter from port 1, and the optical ISO is used to prevent the reflection of ASE from the Sagnac filter. The measured transmission spectra of the Sagnac filter are illustrated in Fig. 2(b), which shows the insertion loss of the Sagnac filter is $\sim$3 dB. The period of the transmission curves is $\sim$19.78 nm, which is consistent with the theory value.

When the phase matching condition is satisfied [34],

$$\Lambda = \lambda / \left(\mathrm{n_{eff,01}} - \mathrm{n_{eff,11}} \right). \tag{2}$$

LPFG written on TMF can convert LP_{01} mode to LP_{11} mode at the resonance wavelength of the LPFG. Λ and λ represent grating period and resonance wavelength respectively. $n_{eff,01}$ and $n_{eff,11}$ denote effective refractive index of LP_{01} mode and LP_{11} mode respectively. The grating period of the LPFG versus resonance wavelength shows a non-monotonic parabolic trend at 1.0 μm band [35]. There is minimum grating period corresponds to one resonance wavelength, and the transmission spectrum of the LPFG presents one resonance dip. When the period is bigger than the minimum period, there will be two resonance wavelengths that correspond to one same period. Accordingly, the transmission spectrum of the LPFG shows two resonance dips. If the grating period is suitable, the two resonance dips will overlap with each other [36], thus an LPFG with broad conversion bandwidth can be fabricated. Our group have fabricated a broadband LPFG with the mode conversion efficiency higher than 93.7% (12 dB) from 940 nm to1065 nm using Corning SMF-28e fiber (NA: 0.14, cutoff wavelength: < 1260 nm, core diameter: 8.2 μm, cladding diameter: 125 μm) [37], which is calculated to be a TMF at 1.0 μm band. The insertion loss of the LPFG is $\sim$1 dB. In the experiment of this paper, the broadband LPFG is employed as a broadband mode converter.

III. EXPERIMENTAL RESULT AND DISCUSSION

When the pump power is 428.3 mW, we adjust PC2 and PC3 properly to achieve mode-locked operation of the laser. Fundamental mode pulse emitted from the polarizer will be converted into LP_{11} mode pulse by the LPFG. And 36% LP_{11} mode pulse launched out from the LPFG is reflected back into the laser
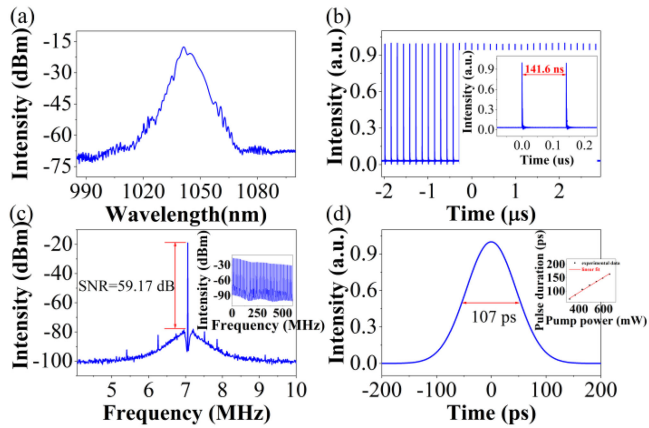
Fig. 3. Output characteristics of mode-locking operation at the wavelength of 1041.361 nm. (a) Output spectrum; (b) Pulse train of the laser with 5 μs time window, inset: pulse with a time duration of 320 ns; (c) RF spectrum of the pulse with a 6 MHz span, inset: RF spectrum with a 600 MHz span; (d) Autocorrelation trace, inset: measured pulse duration versus pump power.
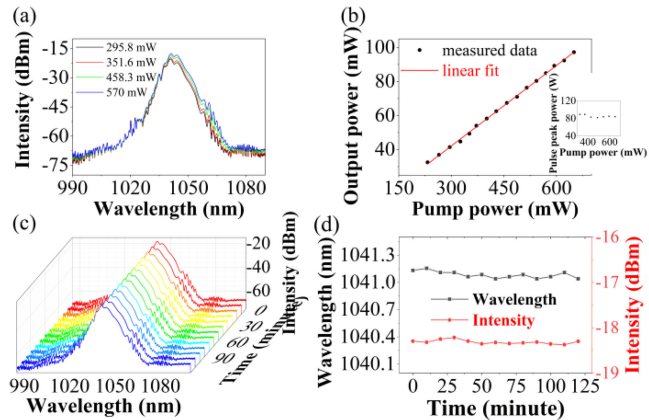

Fig. 4. (a) Output spectra under different pump power; (b) Output power as a function of pump power, inset: pulse peak power versus pump power; (c) Output spectra recorded with intervals of 10 minutes during 2 hours under the pump power of 428.3 mW; (d) Center wavelength and intensity variation during 2 hours with the pump power of 428.3 mW.

TABLE I
SOME PREVIOUS WORKS ABOUT ALL-FIBER MODE-LOCKED CVB LASERS

Methods	Slop efficiency	Maximum output power	Pulse duration	Fundamental repetition rate	Reference
Offset Splicing + FBG	1.4%	~2.4 mW	2.8 ns-23 ns	0.67 MHz	[17]
LPFG + FBG	10.24%	~21.5 mW	6 ns	15.65 MHz	[18]
MSC	3.6%	~3.3 mW	Not metioned	18.58 MHz	[19]
TMF-OC	0.22%	~1 mW	2.552 ps	3.96 MHz	[20]
Offset Splicing + FBG + Mode Superposition	1.5%	~4.67 mW	74.82 ps	40.83 MHz	[21]
LPFG	15.75%	97.2 mW	71 ps-164 ps-	7.06 MHz	This work

changes, the output power is measured by using a power meter (Tgorlabs, S146C, 900 nm-1650 nm, 20 W). Fig. 4(b) indicates the slope efficiency is as high as 15.75% with the mode-locking threshold value of 232.5 mW. The inset of Fig. 4(b) shows the pulse peak power is between 83.95 W and 89.18 W when the pump power varies from 326.2 mW to 650 mW. Table I lists some previous works about all-fiber mode-locked CVB fiber lasers. It can be seen our laser has the highest slope efficiency and largest output power, which is attributed to the dumbbell-shaped configuration and the high transmissivity of the output cavity mirror. To evaluate the mode-locking stability, the output spectra are recorded every 10 minutes in 2 hours at room temperature under the pump power of 428.3 mW. As depicted in Fig. 4(c), the change of the spectral profile is almost negligible. Fig. 4(d) shows the fluctuations of center wavelength and power are less than 0.12 nm and 0.16 dB within 2 hours. In addition, the SNR of the RF spectrum is larger than 59 dB and the pulses possess a highly uniform amplitude. These indicate the mode-locked operation is very stable.

Keeping the polarization state of PC1 and adjusting PC2 and PC3, the central wavelength can be tuned within ~3 nanometers due to the effect of intra-cavity birefringence filtering. Changing the polarization state of PC1 in the Sagnac filter under the pump power of 428.3 mW, the filter spectrum of the Sagnac filter will change accordingly and the gains and losses of different wavelengths are balanced. As depicted in Fig. 5, the central wavelength is continuously tuned from 1023.257 nm to 1046.123 nm corresponding to a tunable range of 22.866 nm with mode-locked operating state. The 3 dB bandwidths and intensity of the spectra are slightly different, which may be caused by the different modulation depth of the transmission curve and different intra-cavity losses with different polarization states of the three PCs. It can be seen that all the side-mode suppression ratios are >43 dB. The spectrum fringes are caused

cavity by the Sagnac reflector, while 64% of which is output. As shown in Fig. 3(a), the central wavelength is 1041.361 nm with the 3 dB linewidth of 2.928 nm. The corresponding pulse train illustrated in Fig. 3(b) shows the pulse interval is 141.6 ns. The radio-frequency (RF) spectrum of the mode-locked pulse train with a 6 MHz span and 30 Hz resolution in Fig. 3(c) indicates the fundamental repetition rate is 7.06 MHz, which matches with the cavity length of 14.60 m. And the SNR at fundamental repetition frequency is 59.17 dB. The inset exhibits a wider RF spectrum with a 600 MHz span and 100 Hz resolution. The autocorrelation curve shown in Fig. 3(d) illustrates the pulse width is 107 ps. The inset of Fig. 3(d) illustrates the pulse duration increases linearly with pump power.

Changing the pump power, the laser can keep at stable mode-locked state and the spectral width is slightly broadened with the increase of pump power due to the enhancement of the nonlinear effect as depicted in Fig. 4(a). When the pump power
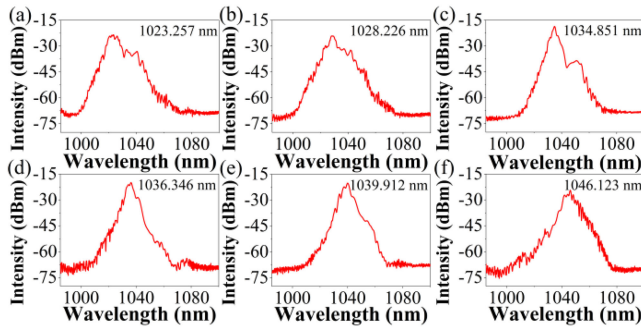
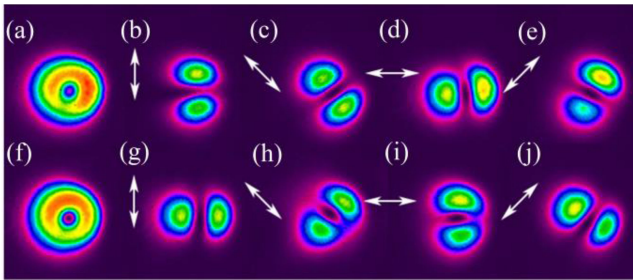Fig. 5.   Output spectra of the laser operating at different central wavelengths.

Fig. 6.   (a) Intensity distribution of radially polarized beam; (b)–(e) Intensity distributions of radially polarized beam after an LP; (f) Intensity distribution of azimuthally polarized beam; (h)–(j) Intensity distributions of azimuthally polarized beam after an LP. The white arrows denote the axis of the LP.

by the interference between LP_{11} mode and a small amount of residual LP_{01} mode which is not transformed.

When the laser operates at mode-locked operating state, adjusting PC4 carefully to remove the degeneracy of the LP_{11} mode, both radially and azimuthally polarized beams can be obtained from the output end. The intensity distributions and images can be observed by a CCD camera. The beam profiles of the radially and azimuthally polarized beams are illustrated in Fig. 6(a) and (f) respectively, presenting a doughnut-shaped intensity profile, which is a typical characteristic of CVBs. Fig. 6(b) to (e) and Fig. 6(g) to (j) show the intensity distributions of radially and azimuthally polarized beams after passing through an LP at different orientations respectively, which conforms to the characteristics of CVBs. Using the bending-loss method proposed in Ref. [38], the mode purity of the CVBs is measured to be 94.86%.

IV. CONCLUSION

In summary, a dumbbell-shaped NPR mode-locked CVB fiber laser with high efficiency was demonstrated. Fundamental frequency mode-locking can be realized by adjusting PCs inside the cavity. The laser can achieve continuously wavelength-tunable mode-locked operation from 1023.257 nm to 1046.123 nm by using a Sagnac filter. At the typical wavelength of 1041.361 nm, the laser delivers CVB pulses with the pulse duration of 107 ps. The slope efficiency is as high as 15.75%. The fundamental repetition rate is 7.06 MHz and the maximum output power is 97.2 mW, corresponding to the pulse energy of 13.8

nJ. The fluctuations of central wavelength and power are less than 0.12 nm and 0.16 dB within 2 hours, which demonstrates the stability of the mode-locking state. The mode purity of the CVBs is 94.86%. It has good application prospects in sensor, optical tweezers, and MDM systems.

REFERENCES

[1] S. Quabis, R. Dorn, M. Eberler, O. Glöckl, and G. Leuchs, "Focusing light to a tighter spot," *Opt. Commun.*, vol. 179, no. 1-6, pp. 1–7, May 2000, doi: 10.1016/S0030-4018(99)00729-4.

[2] Q. Zhan and J. R. Leger, "Focus shaping using cylindrical vector beams," *Opt. Exp.*, vol. 10, no. 7, pp. 324–331, Apr. 2002, doi: 10.1364/OE.10.000324.

[3] C. Xu, K. Yan, C. Gu, P. Yao, L. Xu, and Q. Zhan, "All-fiber laser with flattop beam output using a few-mode fiber Bragg grating," *Opt. Lett.*, vol. 43, no. 6, pp. 1247–1250, Mar. 2018, doi: 10.1364/OL.43.001247.

[4] M. Meier, V. Romano, and T. Feurer, "Material processing with pulsed radially and azimuthally polarized laser radiation," *Appl. Phys. A*, vol. 86, pp. 329–334, Dec. 2007, doi: 10.1007/s00339-006-3784-9.

[5] L. Huang, H. Guo, J. Li, L. Ling, B. Feng, and Z. Y. Li, "Optical trapping of gold nanoparticles by cylindrical vector beam," *Opt. Lett.*, vol. 37, no. 10, pp. 1694–1696, May 2012, doi: 10.1364/ol.37.001694.

[6] X. Wang, Z. Zeng, X. Zhuang, F. Wackenhut, A. Pan, and A. J. Meixner, "Second-harmonic generation in single cdse nanowires by focused cylindrical vector beams," *Opt. Lett.*, vol. 42, no. 13, pp. 2623–2626, Jul. 2017, doi: 10.1364/OL.42.002623.

[7] E. Skoulas, A. Manousaki, C. Fotakis, and E. Stratakis, "Biomimetic surface structuring using cylindrical vector femtosecond laser beams," *Sci. Rep.*, vol. 7, Mar. 2017, Art. no. 45114, doi: 10.1038/srep45114.

[8] M. Xian, Y. Xu, X. Ouyang, Y. Cao, S. Lan, and X. Li, "Segmented cylindrical vector beams for massively-encoded optical data storage," *Sci. Bull.*, vol. 65, no. 24, pp. 2072–2079, Jul. 2020, doi: 10.1016/j.scib.2020.07.016.

[9] J. Yang *et al.*, "Cylindrical vector modes based Mach-Zehnder interferometer with vortex fiber for sensing applications," *Appl. Phys. Lett.*, vol. 115, no. 5, Jul. 2019, Art. no. 051103, doi: 10.1063/1.5109604.

[10] F. Alsolamy, W. A. Alomar, and A. Grbic, "Cylindrical vector beams for wireless power transfer," *IEEE Trans. Antennas Propag.*, vol. 69, no. 3, pp. 1716–1727, Mar. 2021, doi: 10.1109/tap.2020.3026428.

[11] M. R. Beversluis, L. Novotny, and S. J. Stranick, "Programmable vector point-spread function engineering," *Opt. Exp.*, vol. 14, no. 7, pp. 2650–2656, Apr. 2006, doi: 10.1364/oe.14.002650.

[12] Z. Bomzon, G. Biener, V. Kleiner, and E. Hasman, "Radially and azimuthally polarized beams generated by space-variant dielectric subwavelength gratings," *Opt. Lett.*, vol. 27, no. 5, pp. 285–287, Mar. 2002, doi: 10.1364/ol.27.000285.

[13] D. lin, N. Baktash, S. U. Alam, and D. J. Richardson, "106W, picosecond Yb-doped fiber MOPA system with a radially polarized output beam," *Opt. Lett.*, vol. 43, no. 20, pp. 4957–4960, Oct. 2018, doi: 10.1364/OL.43.004957.

[14] R. Zhou, J. W. Haus, P. E. Powers, and Q. Zhan, "Vectorial fiber laser using intracavity axial birefringence," *Opt. Exp.*, vol. 18, no. 10, pp. 10839–10847, May 2010, doi: 10.1364/oe.18.010839.

[15] J. L. Li, K. I. Ueda, M. Musha, A. Shirakawa, and L. X. Zhong, "Generation of radially polarized mode in yb fiber laser by using a dual conical prism," *Opt. Lett.*, vol. 31, no. 20, pp. 2969–2971, Oct. 2010, doi: 10.1364/ol.31.002969.

[16] X. Chen, S. Liu, Z. Lin, Z. Chen, and J. Pu, "Dual-cavity digital laser for intra-cavity mode shaping and polarization control," *Opt. Exp.*, vol. 26, no. 14, pp. 18182–18189, Jul. 2018, doi: 10.1364/OE.26.018182.

[17] B. Sun *et al.*, "Mode-locked all-fiber laser producing radially polarized rectangular pulses," *Opt. Lett.*, vol. 40, no. 8, pp. 1691–1694, Apr. 2015, doi: 10.1364/ol.40.001691.

[18] R. S. Chen *et al.*, "Mode-locked all-fiber laser generating optical vortex pulses with tunable repetition rate," *Appl. Phys. Lett.*, vol. 112, no. 26, Jun. 2018, Art. no. 261103, doi: 10.1063/1.5039566.

[19] H. Wan, J. Wang, Z. Zhang, J. Wang, S. Ruan, and L. Zhang, "Passively mode-locked ytterbium-doped fiber laser with cylindrical vector beam generation based on mode selective coupler," *J. Lightw. Technol.*, vol. 36, no. 16, pp. 3403–3407, Aug. 2018, doi: 10.1109/jlt.2018.2840489.

[20] Y. Xu, S. Chen, Z. Wang, B. Sun, H. Wan, and Z. Zhang, "Cylindrical vector beam fiber laser with a symmetric two-mode fiber coupler," *Photon. Res.*, vol. 7, no. 12, pp. 1479–1484, Dec. 2019, doi: 10.1364/PRJ.7.001479.

[21] C. Dai *et al.*, "Mode-locked fiber laser generating cylindrical vector beams based on an all-polarization-maintaining fiber structure," *Opt. Laser Technol.*, vol. 146, Oct. 2022, Art. no. 107592, doi: 10.1016/j.optlastec.2021.107592.

[22] G. F. Pérez-García, J. L. Camas-Anzueto, G. Anzueto-Sánchez, M. Pérez-Patricio, and F. R. López-Estrada, "Demonstration of improving the sensitivity of a fiber optic temperature sensor using the wavelength of maximum absorption of the lophine," *Measurement*, vol. 187, Oct. 2022, Art. no. 110378, doi: 10.1016/j.measurement.2021.110378.

[23] J. Cao, Y. Sun, Y. Kong, and W. Qian, "The sensitivity of grating-based SPR sensors with wavelength interrogation," *Sensors*, vol. 19, no. 2, Jan. 2019, Art. no. 405, doi: 10.3390/s19020405.

[24] D. Vojna *et al.*, "Verdet constant of potassium terbium fluoride crystal as a function of wavelength and temperature," *Opt. Lett.*, vol. 45, no. 7, pp. 1683–1686, Apr. 2020, doi: 10.1364/OL.387911.

[25] R. Diebolder, C. U. Schmid, R. G. Luthardt, H. Rudolph, and K. Kuhn, "Characterization of the transmission behavior of dental filling materials and cements for the diode lasers' and the Nd:YAG laser's wavelengths," *Lasers Surg. Med.*, vol. 51, no. 7, pp. 653–663, Mar. 2019, doi: 10.1002/lsm.23081.

[26] G. Leitz, E. Fa ̈llman, S. Tuck, and O. Axner, "Stress response in caenorhabditis elegans caused by optical tweezers: Wavelength, power, and time dependence," *Biophys. J.*, vol. 82, no. 4, pp. 2224–2231, Apr. 2002, doi: 10.1016/s0006-3495(02)75568-9.

[27] Q. Rong, Y. Wang, Z. Shao, and X. Qiao, "Large diameter fiber-optics tweezers for escherichia coli bacteria manipulation," *IEEE J. Sel. Top. Quantum Electron.*, vol. 25, no. 2, Mar. 2019, Art. no. 7101807, doi: 10.1109/jstqe.2018.2873203.

[28] Z. Wu, D. Liu, S. Fu, L. Li, M. Tang, and L. Zhao, "Scalar-vector soliton fiber laser mode-locked by nonlinear polarization rotation," *Opt. Exp.*, vol. 24, no. 16, pp. 18764–18771, Aug. 2016, doi: 10.1364/OE.24.018764.

[29] Y. Meng, M. Salhi, A. Niang, K. Guesmi, G. Semaan, and F. Sanchez, "Mode-locked Er:Yb-doped double-clad fiber laser with 75-nm tuning range," *Opt. Lett.*, vol. 40, no. 7, pp. 1153–1156, Apr. 2015, doi: 10.1364/OL.40.001153.

[30] S. D. Emami, M. M. Dashtabi, H. J. Lee, A. S. Arabanian, and H. A. A. Rashid, "1700 nm and 1800 nm band tunable thulium doped mode-locked fiber lasers," *Sci. Rep.*, vol. 7, Oct. 2017, Art. no. 12747, doi: 10.1038/s41598-017-13200-x.

[31] T. Wang, W. Ma, Q. Jia, Q. Su, P. Liu, and P. Zhang, "Passively mode-locked fiber lasers based on nonlinearity at 2-μm band," *IEEE J. Sel. Top. Quantum Electron.*, vol. 24, no. 3, Jun. 2018, Art. no. 1102011, doi: 10.1109/JSTQE.2017.2783047.

[32] N. J. Doran and D. Wood, "Nonlinear-optical loop mirror," *Opt. Lett.*, vol. 13, no. 1, pp. 56–58, Jan. 1988, doi: 10.1364/ol.13.000056.

[33] K. L. Lee, M. P. Fok, S. M. Wan, and C. Shu, "Optically controlled sagnac loop comb filter," *Opt. Exp.*, vol. 12, no. 25, pp. 6335–6340, Dec. 2004, doi: 10.1364/opex.12.006335.

[34] T. Erdogan, "Fiber grating spectra," *J. Lightw. Technol.*, vol. 15, no. 8, pp. 1277–1294, Aug. 1997, doi: 10.1109/50.618322.

[35] Y. Guo *et al.*, "More than 110-nm broadband mode converter based on dual-resonance coupling mechanism in long period fiber gratings," *Opt. Laser Technol.*, vol. 118, pp. 8–12, May 2019, doi: 10.1016/j.optlastec.2019.04.039.

[36] X. Zhao, Y. Liu, Z. Liu, and C. Mou, "All-fiber bandwidth tunable ultra-broadband mode converters based on long-period fiber gratings and helical long-period gratings," *Opt. Exp.*, vol. 28, no. 8, pp. 11990–12000, Apr. 2020, doi: 10.1364/oe.389471.

[37] R. Tao, X. Li, Y. Zhang, and P. Yao, "All-fiber mode-locked laser emitting broadband-spectrum cylindrical vector mode," *Opt. Laser Technol.*, vol. 113, Nov. 2020, Art. no. 105945, doi: 10.1016/j.optlastec.2019.105945.

[38] B. Sun *et al.*, "Low-threshold single-wavelength all-fiber laser generating cylindrical vector beams using a few-mode fiber Bragg grating," *Opt. Lett.*, vol. 37, no. 4, pp. 464–466, Feb. 2012, doi: 10.1364/ol.37.000464.